Momentum-Resolved Exciton Coupling and Valley Polarization Dynamics in Monolayer WS_2

Alice Kunin,[1] Sergey Chernov,[1] Jin Bakalis,[1] Ziling Li,[2] Shuyu Cheng,[2] Zachary H. Withers,[3] Michael G. White,[1,4] Gerd Schönhense,[5] Xu Du,[3] Roland K. Kawakami,[2] and Thomas K. Allison[1,3,*]

[1]*Department of Chemistry, Stony Brook University, Stony Brook, New York 11794, USA*
[2]*Department of Physics, The Ohio State University, Columbus, Ohio 43210, USA*
[3]*Department of Physics and Astronomy, Stony Brook University, Stony Brook, New York 11794, USA*
[4]*Chemistry Division, Brookhaven National Laboratory, Upton, New York 11973, USA*
[5]*Johannes Gutenberg-Universität, Institut für Physik, D-55099 Mainz, Germany*

(Received 14 March 2022; accepted 22 December 2022; published 27 January 2023)

Using time- and angle-resolved photoemission, we present momentum- and energy-resolved measurements of exciton coupling in monolayer WS_2. We observe strong intravalley coupling between the B_{1s} exciton and $A_{n>1}$ states. Our measurements indicate that the dominant valley depolarization mechanism conserves the exciton binding energy and momentum. While this conservation is consistent with Coulomb exchange-driven valley depolarization, we do not observe a momentum or energy dependence to the depolarization rate as would be expected for the exchange-based mechanism.

DOI: 10.1103/PhysRevLett.130.046202

Monolayer transition metal dichalcogenides (TMDs) have garnered sustained interest over the last 10 years following the discovery of valley-selective circular dichroism in these novel, atomically thin, direct band gap semiconductors [1–8]. Right (σ^+) and left (σ^-) circularly polarized light selectively excites interband transitions in the inequivalent K^+ and K^- valleys, respectively, where the band extrema are located [9,10]. Strong Coulomb forces and spin-orbit coupling in these materials yield two series of tightly bound exciton states of opposite spin character in each K valley, the A and B excitons, giving rise to the potential for long-lived, spin-valley locked excitons [11–16]. These unique excitons provide a promising platform for novel optoelectronic and valleytronic device applications [17–22].

In TMD monolayers, the same strong Coulomb forces that give exciton binding energies on the order of ~0.5 eV [23,24] also give rise to substantial interactions between exciton states, both within the same valley (*intravalley* coupling) and between different valleys (*intervalley* coupling). The Coulomb exchange interaction couples bright excitons of opposite spin character, coupling A and B excitons within the same valley ($A^+ \leftrightarrow B^+$) or degenerate excitons in opposite valleys ($A^+ \leftrightarrow A^-$, $B^+ \leftrightarrow B^-$) although its strength and thus its contribution to valley depolarization is disputed among theoretical models [25–33]. The intervalley direct Coulomb interaction couples excitons of the same spin character in the opposite valleys ($A^+ \leftrightarrow B^-$, $B^+ \leftrightarrow A^-$) and has been recently proposed to be more efficient than exchange-based coupling [34–38]. The additional role of exciton-phonon interactions in both intervalley and intravalley exciton dynamics is also non-negligible [39–42].

While these dynamics are formulated in momentum space, previous experiments have been momentum integrated. Many optical spectroscopy techniques have been employed to investigate valley lifetimes and depolarization mechanisms in monolayer TMDs, including photoluminescence [5,43–46], differential transmission [34,47], time-resolved Kerr and Faraday rotation [48–55], and multidimensional spectroscopies [32,56–59], among others [60]. Valley polarization lifetimes ranging from a few picoseconds [34,44,45] to hundreds [47,49,51] or tens [58] of femtoseconds have been reported, depending on the system under study and the spectroscopy method. Interpreting this body of work has been the subject of considerable debate [34,36,58,61–63]. In addition to being momentum-integrated, optical measurements can only probe bright states, and thus only see a subset of the exciton states involved in the dynamics. Optical measurements can also only distinguish between different excitons via the excitation energy and polarization selection rules. Recently, technological advancements in time- and angle-resolved photoemission spectroscopy (tr-ARPES) have enabled the first time-resolved momentum-space measurements on small monolayer TMD samples [64–68]. However, the momentum-resolved exciton dynamics after valley-polarized excitation have yet to be investigated.

In this Letter, we employ tr-ARPES with valley-selective excitation to probe the dynamics of ultrafast exciton coupling and depolarization in monolayer WS_2. Our approach yields momentum-resolved images of the exciton dynamics across the full Brillouin zone following excitation with circularly and linearly polarized light at the nominal B exciton resonance at 2.4 eV [69]. The initially

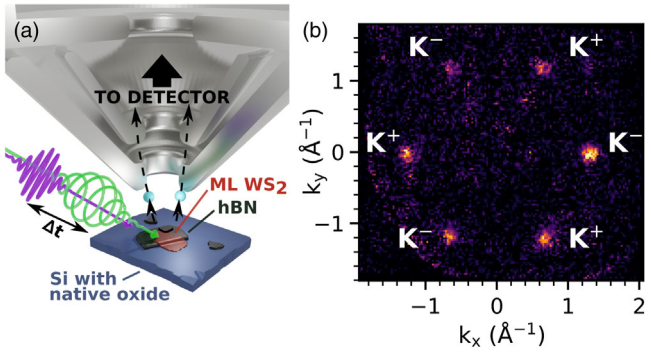

FIG. 1. Time-resolved ARPES of excitons in monolayer WS_2. (a) Linearly or circularly polarized pump pulses excite the sample, and a time-delayed XUV probe pulse photoejects electrons that are extracted into the momentum microscope. (b) Raw exciton signal at 210 fs delay ($h\nu_{\mathrm{probe}} = 25.2$ eV).

excited photoemission signals reveal the direct formation of a mixture of $A_{n>1}$ and B_{1s} excitons due to intravalley coupling, similar in character but larger in magnitude than recently predicted by Guo *et al.* [57]. Following valley-selective excitation, we observe that rapid valley depolarization conserves the unrelaxed exciton binding energy and momentum distributions, consistent with depolarization driven by intervalley Coulomb exchange and inconsistent with other proposed mechanisms involving the direct Coulomb interaction or phonon scattering. These are the first reported measurements of these dynamics that encompass signals from all involved exciton states, both bright and dark.

Linearly or circularly polarized pump pulses ($h\nu_{\mathrm{pump}} = 2.4$ eV) and *p*-polarized extreme ultraviolet (XUV) probe pulses ($h\nu_{\mathrm{probe}} = 20$–$30$ eV) with variable delay illuminate the sample and photoelectrons are collected by a custom time-of-flight momentum microscope [Fig. 1(a)] [70–72]. High data rates are enabled by conducting the experiment at 61 MHz repetition rate with XUV probe pulses produced via cavity-enhanced high-harmonic generation [73–75]. The sample is an exfoliated $\sim 10 \times 10$ μm^2 monolayer of WS_2 stacked on an exfoliated buffer layer of hexagonal boron nitride on a silicon substrate. The energy resolution is broadened to approximately 160 meV due to sample inhomogeneity, but the spin-orbit splitting of the valence bands at the *K* valley is still clearly resolved [64,76]. Additional sample characterization and experimental details can be found in the Supplemental Material [76]. All measurements are done at room temperature unless stated otherwise.

The 2.4 eV pump pulses produce photoexcited signals at the *K* valleys [Fig. 1(b)]. By varying the excitation fluence between 1.3 and 29 $\mu J/cm^2$, we find the tr-ARPES signals are fluence independent below 5 $\mu J/cm^2$ [76]. Thus, all measurements reported here are conducted at 5 $\mu J/cm^2$ excitation fluence, corresponding to an excitation density of approximately 7×10^{11} carriers/cm^2 at our pump energy [69]. Crucially, this low excitation density results in the formation of bound excitons, as opposed to densities near or above the Mott transition [85–89]. The cross-correlation of the pump and probe pulses yields a Gaussian instrument response function with 200 ± 20 fs FWHM.

Photoexcitation with linearly polarized light populates the K^+ and K^- valleys equally and both valleys show the same dynamics. The time-resolved photoelectron spectrum (TRPES) recorded with *s*-polarized excitation is shown in Fig. 2. In tr-ARPES spectra, exciton signals appear within the band gap below the conduction band due to the exciton binding energy [64,90,91] [Figs. 2(a) and 2(b)]. The energy scale of the data in Fig. 2(c) is referenced to the valence band maximum (VBM), which we directly measure in our experiment, with the corresponding binding energy scale shown alongside in Fig. 2(b). No intensity is ever observed

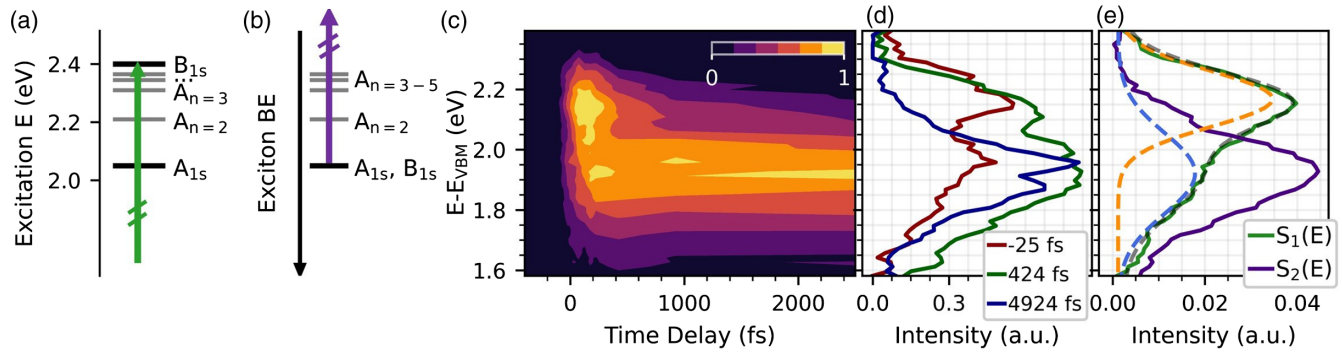

FIG. 2. Excitons formed by linearly polarized excitation. (a) The 2.4 eV pump pulses are resonant with the *B* exciton of WS_2. Excitation energies are derived from [23,24,69]. (b) In our tr-ARPES spectra, the exciton signals are separated by exciton binding energy, with lower binding energies appearing at higher energies above the VBM. (c) The TRPES of the *K*-valley signals following *s*-polarized photoexcitation, (d) energy distribution curves for selected time points, and (e) two-component GA spectral components show a prompt, short-lived feature centered at higher energies [$S_1(E)$] and a long-lived lower energy feature [$S_2(E)$]. A double Gaussian fit of S_1(E) (yellow and blue dashed lines, total fit in gray dashed line) implies the distribution of lower binding energy population comprises approximately $50 \pm 10\%$ of the total intensity in $S_1(E)$. $h\nu_{\mathrm{probe}} = 25.2$ eV.

in the conduction band at $E_{\mathrm{VBM}} + h\nu_{\mathrm{pump}} = 2.4$ eV, indicating the direct formation of bound excitons. The most prominent feature at early pump-probe delays is the large intensity at energies between 2.05–2.3 eV above the VBM in the K valley [Fig. 2(d)]. This corresponds to exciton binding energies compatible with excited A excitons ($A_{n>1}$) [23,24]. At longer delays, a lower energy feature centered at approximately 1.93 eV grows in and persists beyond the longest pump-probe delays recorded (25 ps). This lower energy feature appears at binding energies compatible with those expected for both the A_{1s} and B_{1s} excitons. The A_{1s} and B_{1s} states are expected to have similar exciton binding energies [92,93], and thus appear at the same energy in the photoelectron spectrum. Further explanation of the exciton appearance energies can be found in the Supplemental Material [76].

The spectrum of Fig. 2(c) consists of multiple overlapping components. To deconvolve the overlapping spectral and temporal components of the experimental data, we have applied global analysis (GA) [94–98], which reduces the signal to a few principal spectral components $S_i(E)$, each with simple exponential time dynamics convolved with the instrument response $f_i(t)$, viz. $I(E,t) = \sum_i^N S_i(E) f_i(t)$. We find an excellent fit with only $N = 2$ components. Component 1 corresponds to the initially excited population and is peaked at $E - E_{\mathrm{VBM}} = 2.15$ eV but also shows a long tail to lower photoelectron energies (larger binding energies) covering the region of the B_{1s} exciton [Fig. 2(e)]. We assign this to an initially excited mixture of $A_{n>1}$ and B_{1s} excitons. Component 1 decays with a time constant of 378 ± 40 fs, giving rise to component 2, which is centered at the energy of the long-delay photoelectron spectrum and has a GA lifetime longer than 50 ps. We assign this long-lived component 2 to the formation of the A_{1s} exciton. We find adding additional components beyond $N = 2$ does not improve the quality of the fit or offer additional physical insight.

Despite initial photoexcitation of the B exciton resonance, we clearly observe strong weighting towards lower binding energies consistent with population of the $A_{n>1}$ excited states. This is seen in both the GA $S_1(E)$ component *and* the raw data. By fitting a double Gaussian function to the initially pumped $S_1(E)$ component, we estimate that approximately $50 \pm 10\%$ of this initial distribution is comprised of $A_{n>1}$ exciton population and $50 \pm 10\%$ is B_{1s} excitons [76]. This indicates very strong mixing of the B_{1s} states with $A_{n>1}$ states, such that photoexcitation of what is nominally the B exciton resonance promptly populates $A_{n>1}$ exciton states as well. Such A/B mixing due to intravalley Coulomb exchange has been discussed before. For example, for monolayer MoS_2, Guo *et al.* [57] calculated that the B_{1s} exciton has 5% of A exciton character. The degree of mixing we observe here for WS_2 is notably much larger. Additional details of the GA decomposition and the Gaussian fitting can be found in the Supplemental Material [76].

The dynamics observed under linearly polarized excitation can be due to a mixture of both intervalley and intravalley relaxation mechanisms. To disentangle their relative contributions, we use circularly polarized pump pulses to prepare valley-polarized excitons. We excite the sample with either σ^+ and σ^- polarizations, which preferentially excite K^+ and K^- valleys, respectively. Figure 3(a) shows the integrated K^- and K^+ valley signals under σ^- photoexcitation. The K^+ and K^- valley signals following s- and σ^+-polarized photoexcitation can be found in the

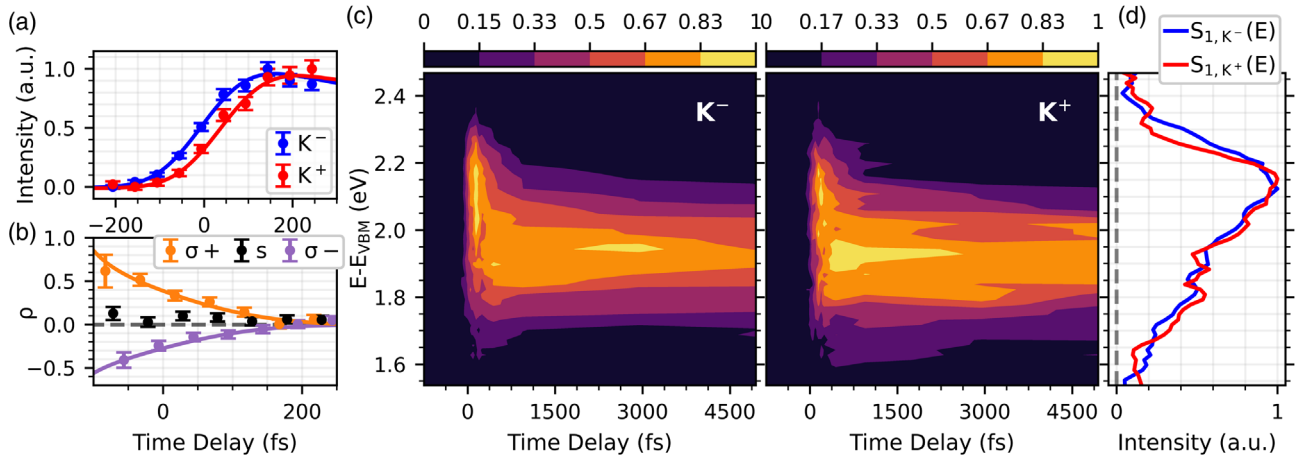

FIG. 3. Excitons formed by σ^- excitation. (a) Integrated intensities for the K^- and K^+ valleys following σ^- excitation. (b) The valley asymmetry (ρ) for σ^+, σ^-, and s-polarized photoexcitation. Points are experimental data, lines are GA fits. The observed valley asymmetry decay timescale of ~250 fs is limited by the instrument response. (c) Comparison of the K^- and K^+ valleys following σ^- excitation shows that the two valleys present nearly identical dynamics, the difference being a 43 ± 4 fs delay in the appearance of signal in the unpumped K^+ valley. $h\nu_{\mathrm{probe}} = 25.2$ eV. (d) The GA spectral components $S_1(E)$ for the K^- and K^+ valley signals show that the population transfer from the pumped valleys to the unpumped valleys does not involve significant changes in the energy distribution.

Supplemental Material [76]. Figure 3(b) shows the valley asymmetry, $\rho(t) = \{[I_{K^+}(t) - I_{K^-}(t)]/[I_{K^+}(t) + I_{K^-}(t)]\}$, where I_{K^+} and I_{K^-} denote the integrated intensity in the K^+ and K^- valleys, respectively. The valley asymmetry decays in approximately 250 fs, limited by the instrument response of 200 fs FWHM. We observe similar valley polarization dynamics in data recorded at 126 K [76], suggesting exciton-phonon coupling is not a main driver of the dynamics. For comparison, we also show the *s*-polarized data in Fig. 3(b), which shows no valley asymmetry.

Figures 3(c) and 3(d) show the TRPES and the $S_1(E)$ GA spectral components for the K^- and K^+ valleys after σ^- excitation, respectively. Strikingly, the spectrum in the unpumped K^+ valley does not show any appreciable difference to that of the initially pumped K^- valley, except an approximately 50 fs delay between the population of the two valleys. We quantify this by applying the same GA described above to the K^+ and K^- valleys independently in the circularly polarized data. For the unpumped valley, we allow for a shift, Δt, in the onset of the time dynamics $f_i(t) \to f_i(t - \Delta t)$. We find the spectral components and exponential rates in the K^+ and K^- valleys to be similar to one another and also to those found under *s*-polarized excitation. The delayed onset captured by Δt was found to be the singular notable difference between the dynamics in the two valleys. From the GA fitting, we find $\Delta t = 43 \pm 4$ fs for σ^- excitation and $\Delta t = 53 \pm 6$ fs for σ^+. This 50 fs shift is also apparent in the integrated signals in Fig. 3(a). As a control, we analyzed the *s*-polarized data in the same way and find $\Delta t = 6 \pm 5$ fs. The small 50 fs shift, indicating very rapid valley depolarization, is consistent with the ~250 fs time scale on which $\rho(t)$ becomes zero when the 200 fs instrument response is considered. The integrated GA fits are also shown as the lines in Figs. 3(a) and 3(b).

Importantly, we find that the prompt valley depolarization observed in the tr-ARPES signal is not accompanied by energy relaxation. This is evident from both the data of Fig. 3(c) as well as the GA analysis in Fig. 3(d), with $S_{1,K^+}(E)$ closely resembling $S_{1,K^-}(E)$. Also, applying the same coarse two-Gaussian fitting used in Fig. 2(c) to the K^+ and $K^- S_1(E)$ components gives the $A_{n>1}/B_{1s}$ ratio in the two valleys to be the same within experimental error ($53:47 \pm 8\%$ in S_{1,K^-}, $50:50 \pm 11\%$ in S_{1,K^+}).

Conservation of energy in the valley depolarization is consistent with depolarization driven by intervalley Coulomb exchange, which couples energetically degenerate bright exciton states in the two valleys, e.g., $A^\pm \leftrightarrow A^\mp$, $B^\pm \leftrightarrow B^\mp$ [26,30]. This is in contrast to the recently proposed nondegenerate intervalley depolarization mechanism that couples $A^\pm \leftrightarrow B^\mp$, $B^\pm \leftrightarrow A^\mp$ via the direct Coulomb interaction [37,38]. The direct mechanism couples excitons of different binding energies (e.g., $B^\pm_{1s} \to A^\mp_{n>1}$). Without the restriction of exciton degeneracy, the distribution of excitons appearing in the unpumped valley via depolarization is determined by the coupling matrix elements and the density of states, both of which vary widely across the initial exciton spectrum. Thus, the replication of the K^- valley spectrum in the K^+ valley observed in Fig. 3 would be highly unlikely. However, we do note that we do not observe the *rate* of valley depolarization to depend strongly on the exciton binding energy. The strength of the exchange interaction is expected to increase as the square of the electron-hole wave function overlap, suggesting $A_{n>1}$ states may depolarize more slowly than 1s excitons [99], but this is not observed in the data. Instead, we find the dynamics at all binding energies to be approximately the same. Furthermore, we find that the valley polarization dynamics are not well described by incoherent rate equations, indicating a partially coherent aspect to the dynamics (i.e., dynamics described by Bloch equations), as discussed in the Supplemental Material [76]. This further supports valley depolarization via intervalley exciton coupling rather than phonon scattering.

The photoelectron momentum distributions for the K^+ and K^- valleys following σ^+ excitation are shown in Fig. 4. We quantify the extent of the distributions as a function of time by fitting the energy-integrated valley signals with a Gaussian, $\exp[-(1/2)|\mathbf{k} - K|^2/(\Delta k)^2]$, and report the standard deviation, Δk. We observe that the initial photoelectron momentum distribution [Fig. 4(a)] encompasses nearly twice the extent of the relaxed photoelectron population at 5 ps delay time [Fig. 4(b)]. The final distribution width of $\Delta k \sim 0.07$ Å^{-1} is commensurate with

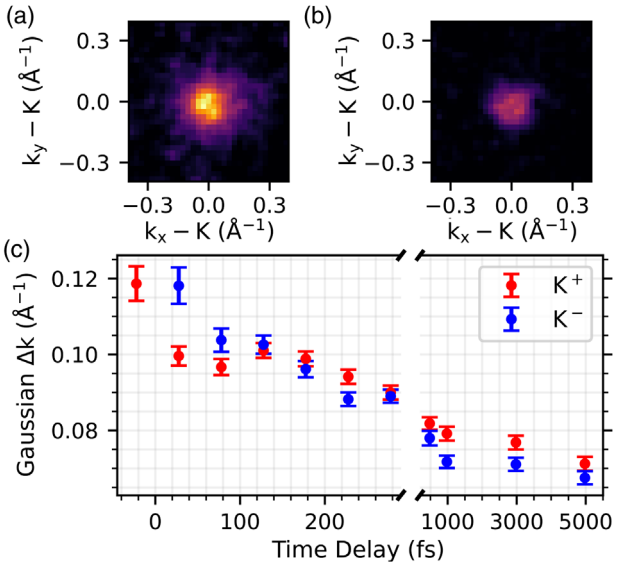

FIG. 4. Time dependence of the photoelectron momentum distributions. Representative images of a K^+ valley at (a) 78 fs and (b) 5 ps after σ^+-polarized photoexcitation. (c) Standard deviation (Δk) of Gaussian distribution fits to the photoelectron momentum distributions in the K^+ and K^- valleys at each delay time after σ^+-polarized photoexcitation ($h\nu_{\text{probe}} = 30$ eV).

the recent experimental measurement of relaxed exciton states of WSe_2 at 90 K [65]. Remarkably, no large differences are observed in the momentum distributions in the K^+ and K^- valleys; the initial K^+ valley distribution with $\Delta k = 0.12$ Å^{-1} arrives at the K^- valley 50 fs later with the same width [Fig. 4(c)].

Valley depolarization driven by the Coulomb exchange interaction is expected to conserve the total exciton momentum $\mathbf{Q} = \mathbf{k}_e - \mathbf{k}_h$. While we do not measure $\mathbf{Q}$ directly in this experiment, we conjecture that the width of the distribution in $\mathbf{Q}$ is correlated with the width of our photoelectron distributions. Thus, the conservation of the photoelectron momentum distribution after intervalley coupling suggests conservation of the exciton momentum, consistent with exchange-driven valley depolarization. However, the strength of the exchange interaction is expected to scale with $|\mathbf{Q}|$, and thus excitons with smaller $\mathbf{Q}$ would be expected to depolarize more slowly. Our results here, however, do not exhibit a difference in the depolarization rate for electrons with different observed $\mathbf{k}_e$.

Finally, we note that previous tr-ARPES work on monolayer WSe_2, excited with linearly polarized light and probed at $h\nu_{\text{probe}} = 21.7$ eV, has emphasized the importance of dark excitons with the electron in the Σ valley (sometimes referred to as Q) [64]. We also observe exciton signals from the Σ valleys in our momentum space images, however we find that these signals depend very strongly on the probe photon energy employed, with many probe photon energies showing no discernible Σ-valley signal (see Supplemental Material [76]). Several features of our data indicate that K-Σ excitons do not play a major role in the valley depolarization dynamics of WS_2. First, the Σ-valley signal we observe appears ∼100 meV higher in photoelectron energy than the K-valley signals, indicating scattering of the electron from K to Σ is an uphill process. This is expected from band-structure calculations in WS_2 [31]. Second, the Σ-valley signal rises concurrently with the pumped K-valley signal and shows a partial decay of ∼215 fs followed by a long-lived component, both much slower than the 50 fs valley depolarization time observed here. If K-Σ excitons played an intermediary role in valley depolarization, one would expect appearance and decay timescales for the Σ signal commensurate with the valley depolarization.

This material is primarily based upon work supported by the U.S. Department of Energy, Office of Science, Office of Basic Energy Sciences under Award No. DE-SC0022004 and the Air Force Office of Scientific Research under FA9550-20-1-0259. R. K. K. acknowledges support from the U.S. National Science Foundation under Grant No. CHE-1935885. X. D. acknowledges support from the U.S. National Science Foundation under Grant No. DMR-1808491. M. G. W. acknowledges support from the U.S. Department of Energy (DOE), Office of Science, Office of Basic Energy Sciences, Chemical Sciences, Geosciences, and Biosciences (CSGB) Division, and the Catalysis Science Program under DOE Contract No. DE-SC0012704. Z. H. W. acknowledges support from the U.S. National Science Foundation Graduate Research Fellowship Program.

*thomas.allison@stonybrook.edu

[1] D. Xiao, W. Yao, and Q. Niu, Phys. Rev. Lett. **99**, 236809 (2007).
[2] W. Yao, D. Xiao, and Q. Niu, Phys. Rev. B **77**, 235406 (2008).
[3] T. Cao, G. Wang, W. Han, H. Ye, C. Zhu, J. Shi, Q. Niu, P. Tan, E. Wang, B. Liu, and J. Feng, Nat. Commun. **3**, 887 (2012).
[4] D. Xiao, G.-B. Liu, W. Feng, X. Xu, and W. Yao, Phys. Rev. Lett. **108**, 196802 (2012).
[5] K. F. Mak, K. He, J. Shan, and T. F. Heinz, Nat. Nanotechnol. **7**, 494 (2012).
[6] H. Zeng, J. Dai, W. Yao, D. Xiao, and X. Cui, Nat. Nanotechnol. **7**, 490 (2012).
[7] G. Kioseoglou, A. T. Hanbicki, M. Currie, A. L. Friedman, D. Gunlycke, and B. T. Jonker, Appl. Phys. Lett. **101**, 221907 (2012).
[8] G. Wang, A. Chernikov, M. M. Glazov, T. F. Heinz, X. Marie, T. Amand, and B. Urbaszek, Rev. Mod. Phys. **90**, 021001 (2018).
[9] G. Sallen, L. Bouet, X. Marie, G. Wang, C. R. Zhu, W. P. Han, Y. Lu, P. H. Tan, T. Amand, B. L. Liu, and B. Urbaszek, Phys. Rev. B **86**, 081301(R) (2012).
[10] G.-B. Liu, W.-Y. Shan, Y. Yao, W. Yao, and D. Xiao, Phys. Rev. B **88**, 085433 (2013).
[11] A. M. Jones, H. Yu, N. J. Ghimire, S. Wu, G. Aivazian, J. S. Ross, B. Zhao, J. Yan, D. G. Mandrus, D. Xiao, W. Yao, and X. Xu, Nat. Nanotechnol. **8**, 634 (2013).
[12] D. Y. Qiu, F. H. da Jornada, and S. G. Louie, Phys. Rev. Lett. **111**, 216805 (2013).
[13] X. Xu, W. Yao, D. Xiao, and T. F. Heinz, Nat. Phys. **10**, 343 (2014).
[14] M. M. Glazov, E. L. Ivchenko, G. Wang, T. Amand, X. Marie, B. Urbaszek, and B. L. Liu, Phys. Status Solidi B **252**, 2349 (2015).
[15] M. Koperski, M. R. Molas, A. Arora, K. Nogajewski, A. O. Slobodeniuk, C. Faugeras, and M. Potemski, Nanophotonics **6**, 1289 (2017).
[16] H.-K. Li, K. Y. Fong, H. Zhu, Q. Li, S. Wang, S. Yang, Y. Wang, and X. Zhang, Nat. Photonics **13**, 397 (2019).
[17] D. Jariwala, V. K. Sangwan, L. J. Lauhon, T. J. Marks, and M. C. Hersam, ACS Nano **8**, 1102 (2014).
[18] J. R. Schaibley, H. Yu, G. Clark, P. Rivera, J. S. Ross, K. L. Seyler, W. Yao, and X. Xu, Nat. Rev. Mater. **1**, 16055 (2016).
[19] K. F. Mak and J. Shan, Nat. Photonics **10**, 216 (2016).
[20] J. Xiao, M. Zhao, Y. Wang, and X. Zhang, Nanophotonics **6**, 1309 (2017).
[21] T. Mueller and E. Malic, npj 2D Mater. Appl. **2**, 29 (2018).
[22] S. A. Vitale, D. Nezich, J. O. Varghese, P. Kim, N. Gedik, P. Jarillo-Herrero, D. Xiao, and M. Rothschild, Small **14**, 1801483 (2018).

[23] A. Chernikov, T. C. Berkelbach, H. M. Hill, A. Rigosi, Y. Li, O. B. Aslan, D. R. Reichman, M. S. Hybertsen, and T. F. Heinz, Phys. Rev. Lett. **113**, 076802 (2014).
[24] H. M. Hill, A. F. Rigosi, C. Roquelet, A. Chernikov, T. C. Berkelbach, D. R. Reichman, M. S. Hybertsen, L. E. Brus, and T. F. Heinz, Nano Lett. **15**, 2992 (2015).
[25] G. E. Pikus and G. L. Bir, Zh. Eksp. Teor. Fiz. **60**, 195 (1971) [Sov. Phys. JETP **33**, 108 (1971)].
[26] H. Yu, G.-B. Liu, P. Gong, X. Xu, and W. Yao, Nat. Commun. **5**, 3876 (2014).
[27] M. M. Glazov, T. Amand, X. Marie, D. Lagarde, L. Bouet, and B. Urbaszek, Phys. Rev. B **89**, 201302(R) (2014).
[28] D. Y. Qiu, T. Cao, and S. G. Louie, Phys. Rev. Lett. **115**, 176801 (2015).
[29] M. M. Glazov, L. E. Golub, G. Wang, X. Marie, T. Amand, and B. Urbaszek, Phys. Rev. B **95**, 035311 (2017).
[30] T. Yu and M. W. Wu, Phys. Rev. B **89**, 205303 (2014).
[31] A. Kormányos, G. Burkard, M. Gmitra, J. Fabian, V. Zólyomi, N. D. Drummond, and V. Falko, 2D Mater. **2**, 022001 (2015).
[32] K. Hao, G. Moody, F. Wu, C. K. Dass, L. Xu, C.-H. Chen, L. Sun, M.-Y. Li, L.-J. Li, A. H. MacDonald, and X. Li, Nat. Phys. **12**, 677 (2016).
[33] G. Moody, J. Schaibley, and X. Xu, J. Opt. Soc. Am. B **33**, C39 (2016).
[34] R. Schmidt, G. Berghäuser, R. Schneider, M. Selig, P. Tonndorf, E. Malić, A. Knorr, S. M. de Vasconcellos, and R. Bratschitsch, Nano Lett. **16**, 2945 (2016).
[35] M. Selig, F. Katsch, R. Schmidt, S. Michaelis de Vasconcellos, R. Bratschitsch, E. Malic, and A. Knorr, Phys. Rev. Res. **1**, 022007(R) (2019).
[36] M. Selig, F. Katsch, S. Brem, G. F. Mkrtchian, E. Malic, and A. Knorr, Phys. Rev. Res. **2**, 023322 (2020).
[37] G. Berghäuser, I. Bernal-Villamil, R. Schmidt, R. Schneider, I. Niehues, P. Erhart, S. M. de Vasconcellos, R. Bratschitsch, A. Knorr, and E. Malic, Nat. Commun. **9**, 971 (2018).
[38] I. Bernal-Villamil, G. Berghäuser, M. Selig, I. Niehues, R. Schmidt, R. Schneider, P. Tonndorf, P. Erhart, S. M. de Vasconcellos, R. Bratschitsch, A. Knorr, and E. Malic, 2D Mater. **5**, 025011 (2018).
[39] Z. Wang, A. Molina-Sánchez, P. Altmann, D. Sangalli, D. D. Fazio, G. Soavi, U. Sassi, F. Bottegoni, F. Ciccacci, M. Finazzi, L. Wirtz, A. C. Ferrari, A. Marini, G. Cerullo, and S. D. Conte, Nano Lett. **18**, 6882 (2018).
[40] M. Selig, G. Berghäuser, M. Richter, R. Bratschitsch, A. Knorr, and E. Malic, 2D Mater. **5**, 035017 (2018).
[41] M. He, P. Rivera, D. V. Tuan, N. P. Wilson, M. Yang, T. Taniguchi, K. Watanabe, J. Yan, D. G. Mandrus, H. Yu, H. Dery, W. Yao, and X. Xu, Nat. Commun. **11**, 618 (2020).
[42] X. Jiang, Q. Zheng, Z. Lan, W. A. Saidi, X. Ren, and J. Zhao, Sci. Adv. **7**, abf3759 (2021).
[43] B. Zhu, H. Zeng, J. Dai, Z. Gong, and X. Cui, Proc. Natl. Acad. Sci. U.S.A. **111**, 11606 (2014).
[44] G. Wang, L. Bouet, D. Lagarde, M. Vidal, A. Balocchi, T. Amand, X. Marie, and B. Urbaszek, Phys. Rev. B **90**, 075413 (2014).
[45] D. Lagarde, L. Bouet, X. Marie, C. R. Zhu, B. L. Liu, T. Amand, P. H. Tan, and B. Urbaszek, Phys. Rev. Lett. **112**, 047401 (2014).
[46] T. Yan, X. Qiao, P. Tan, and X. Zhang, Sci. Rep. **5**, 15625 (2015).
[47] C. Mai, Y. G. Semenov, A. Barrette, Y. Yu, Z. Jin, L. Cao, K. W. Kim, and K. Gundogdu, Phys. Rev. B **90**, 041414(R) (2014).
[48] C. R. Zhu, K. Zhang, M. Glazov, B. Urbaszek, T. Amand, Z. W. Ji, B. L. Liu, and X. Marie, Phys. Rev. B **90**, 161302 (R) (2014).
[49] S. Dal Conte, F. Bottegoni, E. A. A. Pogna, D. De Fazio, S. Ambrogio, I. Bargigia, C. D'Andrea, A. Lombardo, M. Bruna, F. Ciccacci, A. C. Ferrari, G. Cerullo, and M. Finazzi, Phys. Rev. B **92**, 235425 (2015).
[50] W.-T. Hsu, Y.-L. Chen, C.-H. Chen, P.-S. Liu, T.-H. Hou, L.-J. Li, and W.-H. Chang, Nat. Commun. **6**, 8963 (2015).
[51] G. Plechinger, P. Nagler, A. Arora, R. Schmidt, A. Chernikov, A. G. del Águila, P. C. Christianen, R. Bratschitsch, C. Schüller, and T. Korn, Nat. Commun. **7**, 12715 (2016).
[52] G. Plechinger, T. Korn, and J. M. Lupton, J. Phys. Chem. C **121**, 6409 (2017).
[53] E. J. McCormick, M. J. Newburger, Y. K. Luo, K. M. McCreary, S. Singh, I. B. Martin, E. J. Cichewicz, B. T. Jonker, and R. K. Kawakami, 2D Mater. **5**, 011010 (2017).
[54] M. Schwemmer, P. Nagler, A. Hanninger, C. Schüller, and T. Korn, Appl. Phys. Lett. **111**, 082404 (2017).
[55] P. Dey, L. Yang, C. Robert, G. Wang, B. Urbaszek, X. Marie, and S. A. Crooker, Phys. Rev. Lett. **119**, 137401 (2017).
[56] C. L. Smallwood and S. T. Cundiff, Laser Photonics Rev. **12**, 1800171 (2018).
[57] L. Guo, M. Wu, T. Cao, D. M. Monahan, Y.-H. Lee, S. G. Louie, and G. R. Fleming, Nat. Phys. **15**, 228 (2019).
[58] L. T. Lloyd, R. E. Wood, F. Mujid, S. Sohoni, K. L. Ji, P.-C. Ting, J. S. Higgins, J. Park, and G. S. Engel, ACS Nano **15**, 10253 (2021).
[59] T. L. Purz, E. W. Martin, P. Rivera, W. G. Holtzmann, X. Xu, and S. T. Cundiff, Phys. Rev. B **104**, L241302 (2021).
[60] F. Mahmood, Z. Alpichshev, Y.-H. Lee, J. Kong, and N. Gedik, Nano Lett. **18**, 223 (2018).
[61] G. Moody, C. K. Dass, K. Hao, C.-H. Chen, L.-J. Li, A. Singh, K. Tran, G. Clark, X. Xu, G. Berghäuser, E. Malic, A. Knorr, and X. Li, Nat. Commun. **6**, 8315 (2015).
[62] G. Kioseoglou, A. T. Hanbicki, M. Currie, A. L. Friedman, and B. T. Jonker, Sci. Rep. **6**, 25041 (2016).
[63] J. Ye, Y. Li, T. Yan, G. Zhai, and X. Zhang, J. Phys. Chem. Lett. **10**, 2963 (2019).
[64] J. Madéo, M. K. L. Man, C. Sahoo, M. Campbell, V. Pareek, E. L. Wong, A. Al-Mahboob, N. S. Chan, A. Karmakar, B. M. K. Mariserla, X. Li, T. F. Heinz, T. Cao, and K. M. Dani, Science **370**, 1199 (2020).
[65] M. K. L. Man, J. Madéo, C. Sahoo, K. Xie, M. Campbell, V. Pareek, A. Karmakar, E. L. Wong, A. Al-Mahboob, N. S. Chan, D. R. Bacon, X. Zhu, M. M. M. Abdelrasoul, X. Li, T. F. Heinz, F. H. da Jornada, T. Cao, and K. M. Dani, Sci. Adv. **7**, eabg0192 (2021).
[66] R. Wallauer, R. Perea-Causin, L. Münster, S. Zajusch, S. Brem, J. Güdde, K. Tanimura, K.-Q. Lin, R. Huber, E. Malic, and U. Höfer, Nano Lett. **21**, 5867 (2021).
[67] O. Karni, E. Barré, V. Pareek, J. D. Georgaras, M. K. L. Man, C. Sahoo, D. R. Bacon, X. Zhu, H. B. Ribeiro,

A. L. O'Beirne, J. Hu, A. Al-Mahboob, M. M. M. Abdelrasoul, N. S. Chan, A. Karmakar, A. J. Winchester, B. Kim, K. Watanabe, T. Taniguchi, K. Barmak, J. Madéo, F. H. da Jornada, T. F. Heinz, and K. M. Dani, Nature (London) **603**, 247 (2022).

[68] D. Schmitt, J. P. Bange, W. Bennecke, A. AlMutairi, G. Meneghini, K. Watanabe, T. Taniguchi, D. Steil, D. R. Luke, R. T. Weitz, S. Steil, G. S. M. Jansen, S. Brem, E. Malic, S. Hofmann, M. Reutzel, and S. Mathias, Nature (London) **608**, 499 (2022).

[69] Y. Li, A. Chernikov, X. Zhang, A. Rigosi, H. M. Hill, A. M. van der Zande, D. A. Chenet, E.-M. Shih, J. Hone, and T. F. Heinz, Phys. Rev. B **90**, 205422 (2014).

[70] S. Chernov, K. Medjanik, C. Tusche, D. Kutnyakhov, S. Nepijko, A. Oelsner, J. Braun, J. Minár, S. Borek, H. Ebert, H. Elmers, J. Kirschner, and G. Schönhense, Ultramicroscopy **159**, 453 (2015).

[71] K. Medjanik, O. Fedchenko, S. Chernov, D. Kutnyakhov, M. Ellguth, A. Oelsner, B. Schönhense, T. R. F. Peixoto, P. Lutz, C.-H. Min, F. Reinert, S. Däster, Y. Acremann, J. Viefhaus, W. Wurth, H. J. Elmers, and G. Schönhense, Nat. Mater. **16**, 615 (2017).

[72] G. Schönhense, K. Medjanik, O. Fedchenko, A. Zymaková, S. Chernov, D. Kutnyakhov, D. Vasilyev, S. Babenkov, H. J. Elmers, P. Baumgärtel, P. Goslawski, G. Öhrwall, T. Grunske, T. Kauerhof, K. von Volkmann, M. Kallmayer, M. Ellguth, and A. Oelsner, J. Synchrotron Radiat. **28**, 1891 (2021).

[73] X. Li, M. A. R. Reber, C. Corder, Y. Chen, P. Zhao, and T. K. Allison, Rev. Sci. Instrum. **87**, 093114 (2016).

[74] C. Corder, P. Zhao, J. Bakalis, X. Li, M. D. Kershis, A. R. Muraca, M. G. White, and T. K. Allison, Struct. Dyn. **5**, 054301 (2018).

[75] C. Corder, P. Zhao, X. Li, M. D. Kershis, M. G. White, and T. K. Allison, in *Proceedings of Laser Applications in Microelectronic and Optoelectronic Manufacturing (LAMOM) XXIII*, edited by B. Neuenschwander, G. Račiukaitis, T. Makimura, and C. P. Grigoropoulos (SPIE, Bellingham, WA, 2018).

[76] See Supplemental Material at http://link.aps.org/supplemental/10.1103/PhysRevLett.130.046202 for experimental details, additional GA spectra, Σ valley dynamics, and temperature-dependent valley asymmetry, which includes Refs. [77–84].

[77] A. Berkdemir, H. R. Gutiérrez, A. R. Botello-Méndez, N. Perea-López, A. L. Elías, C.-I. Chia, B. Wang, V. H. Crespi, F. López-Urías, J.-C. Charlier, H. Terrones, and M. Terrones, Sci. Rep. **3**, 1755 (2013).

[78] R. Saito, Y. Tatsumi, S. Huang, X. Ling, and M. S. Dresselhaus, J. Phys. Condens. Matter **28**, 353002 (2016).

[79] M. K. L. Man, S. Deckoff-Jones, A. Winchester, G. Shi, G. Gupta, A. D. Mohite, S. Kar, E. Kioupakis, S. Talapatra, and K. M. Dani, Sci. Rep. **6**, 20890 (2016).

[80] A. Steinhoff, M. Florian, M. Rösner, G. Schönhoff, T. O. Wehling, and F. Jahnke, Nat. Commun. **8**, 1166 (2017).

[81] G. Wang, C. Robert, M. M. Glazov, F. Cadiz, E. Courtade, T. Amand, D. Lagarde, T. Taniguchi, K. Watanabe, B. Urbaszek, and X. Marie, Phys. Rev. Lett. **119**, 047401 (2017).

[82] J. P. Echeverry, B. Urbaszek, T. Amand, X. Marie, and I. C. Gerber, Phys. Rev. B **93**, 121107(R) (2016).

[83] A. I. Prazdnichnykh, M. M. Glazov, L. Ren, C. Robert, B. Urbaszek, and X. Marie, Phys. Rev. B **103**, 085302 (2021).

[84] M. Baranowski, A. Surrente, D. K. Maude, M. Ballottin, A. A. Mitioglu, P. C. M. Christianen, Y. C. Kung, D. Dumcenco, A. Kis, and P. Plochocka, 2D Mater. **4**, 025016 (2017).

[85] A. G. Čabo, J. A. Miwa, S. S. Grønborg, J. M. Riley, J. C. Johannsen, C. Cacho, O. Alexander, R. T. Chapman, E. Springate, M. Grioni, J. V. Lauritsen, P. D. C. King, P. Hofmann, and S. Ulstrup, Nano Lett. **15**, 5883 (2015).

[86] S. Ulstrup, A. G. Čabo, D. Biswas, J. M. Riley, M. Dendzik, C. E. Sanders, M. Bianchi, C. Cacho, D. Matselyukh, R. T. Chapman, E. Springate, P. D. C. King, J. A. Miwa, and P. Hofmann, Phys. Rev. B **95**, 041405(R) (2017).

[87] F. Liu, M. E. Ziffer, K. R. Hansen, J. Wang, and X. Zhu, Phys. Rev. Lett. **122**, 246803 (2019).

[88] H. Beyer, G. Rohde, A. G. Čabo, A. Stange, T. Jacobsen, L. Bignardi, D. Lizzit, P. Lacovig, C. E. Sanders, S. Lizzit, K. Rossnagel, P. Hofmann, and M. Bauer, Phys. Rev. Lett. **123**, 236802 (2019).

[89] W. Lee, Y. Lin, L.-S. Lu, W.-C. Chueh, M. Liu, X. Li, W.-H. Chang, R. A. Kaindl, and C.-K. Shih, Nano Lett. **21**, 7363 (2021).

[90] A. Rustagi and A. F. Kemper, Phys. Rev. B **97**, 235310 (2018).

[91] D. Christiansen, M. Selig, E. Malic, R. Ernstorfer, and A. Knorr, Phys. Rev. B **100**, 205401 (2019).

[92] A. V. Stier, K. M. McCreary, B. T. Jonker, J. Kono, and S. A. Crooker, Nat. Commun. **7**, 10643 (2016).

[93] F. Katsch, M. Selig, and A. Knorr, 2D Mater. **7**, 015021 (2019).

[94] I. H. van Stokkum, D. S. Larsen, and R. van Grondelle, Biochim. Biophys. Acta Bioenerg. **1657**, 82 (2004).

[95] C. Z. Bisgaard, O. J. Clarkin, G. Wu, A. M. D. Lee, O. Geßner, C. C. Hayden, and A. Stolow, Science **323**, 1464 (2009).

[96] W. Jin, F. Rupp, K. Chevalier, M. M. N. Wolf, M. C. Rojas, G. Lefkidis, H.-J. Krüger, R. Diller, and W. Hübner, Phys. Rev. Lett. **109**, 267209 (2012).

[97] J. S. Beckwith, C. A. Rumble, and E. Vauthey, Int. Rev. Phys. Chem. **39**, 135 (2020).

[98] M. Rebholz, T. Ding, V. Despré, L. Aufleger, M. Hartmann, K. Meyer, V. Stooß, A. Magunia, D. Wachs, P. Birk, Y. Mi, G. D. Borisova, C. C. Castanheira, P. Rupprecht, G. Schmid, K. Schnorr, C. D. Schröter, R. Moshammer, Z.-H. Loh, A. R. Attar, S. R. Leone, T. Gaumnitz, H. J. Wörner, S. Roling, M. Butz, H. Zacharias, S. Düsterer, R. Treusch, G. Brenner, J. Vester, A. I. Kuleff, C. Ott, and T. Pfeifer, Phys. Rev. X **11**, 031001 (2021).

[99] S.-Y. Chen, T. Goldstein, J. Tong, T. Taniguchi, K. Watanabe, and J. Yan, Phys. Rev. Lett. **120**, 046402 (2018).